

RESEARCH ARTICLE

A biocompatible double-crosslinked gelatin/sodium alginate/dopamine/quaternized chitosan hydrogel for wound dressings based on 3D bioprinting technology

Yueqi Lu^{1,2}, Jie Xu^{1,2}, Ya Su¹, Huan Fang^{1,2}, Jiaqi Liu¹, Siyao Lv¹, Yuen Yee Cheng³, Yi Nie^{2*}, Wenfang Li^{4*}, Bo Pan^{5*}, Kedong Song^{1*}

¹State Key Laboratory of Fine Chemicals, Dalian R&D Center for Stem Cell and Tissue Engineering, Dalian University of Technology, Dalian 116024, China

²Zhengzhou Institute of Emerging Industrial Technology, Zhengzhou 450000, China

³Institute for Biomedical Materials and Devices, Faculty of Science, University of Technology Sydney, NSW 2007, Australia

⁴School of Life Science and Technology, Weifang Medical University, Weifang, 261053, China

⁵Department of Breast Surgery, The Second Hospital of Dalian Medical University, Dalian 116023, China

(This article belongs to the *Special Issue: Novel Nanoencapsulation and Bio-Printing Technologies for Drug Administration*)

***Corresponding authors:**

Kedong Song
(Kedongsong@dlut.edu.cn)

Yi Nie
(ynie@ipe.ac.cn)

Wenfang Li
(liwenfang@wfmuc.edu.cn)

Bo Pan
(dmupanbo@hotmail.com)

Citation: Lu Y, Xu J, Su Y, et al., 2023, A biocompatible double-crosslinked gelatin/sodium alginate/dopamine/quaternized chitosan hydrogel for wound dressings based on 3D bioprinting technology. *Int J Bioprint*.
<https://doi.org/10.18063/ijb.689>

Received: October 25, 2022

Accepted: December 15, 2022

Published Online: February 20, 2023

Copyright: © 2023 Author(s). This is an Open Access article distributed under the terms of the Creative Commons Attribution License, permitting distribution and reproduction in any medium, provided the original work is properly cited.

Publisher's Note: Whioce Publishing remains neutral with regard to jurisdictional claims in published maps and institutional affiliations.

Abstract

Severe skin injuries can cause serious problems, which could affect the patient's normal life, if not dealt properly in a timely and effective manner. It is an urgent requirement to develop personalized wound dressings with excellent antibacterial activity and biocompatibility to match the shape of the wound to facilitate clinical application. In this study, a bioink (GAQ) based on gelatin (Gel)/sodium alginate (SA)/quaternized chitosan (QCS) was prepared, and GAQ hydrogel dressing grafting with dopamine (GADQ) was fabricated by an extrusion three-dimensional (3D) printing technology. QCS was synthesized by modifying quaternary ammonium group on chitosan, and its structure was successfully characterized by nuclear magnetic resonance (1H NMR) and Fourier-transform infrared spectroscopy (FT-IR). Our results showed that the GADQ hydrogel dressing that was double-crosslinked by EDC/NHS and Ca²⁺ had good tensile strength, considerable swelling ratio, and effective antioxidation properties. It also showed that GADQ1.5% had 93.17% and 91.06% antibacterial activity against *Staphylococcus aureus* and *Escherichia coli*, respectively. Furthermore, the relative survival ratios of fibroblast cells seeded on these hydrogels exceeded 350% after cultured for 7 days, which proved the biocompatibility of these hydrogels. Overall, this advanced 3D-printed GADQ1.5% hydrogels with effective antioxidation, excellent antibacterial activity and good biocompatibility had a considerable application potential for wound healing.

Keywords: Quaternized chitosan; 3D bioprinting; Dopamine; Hybrid scaffold; Wound dressings

1. Introduction

Skin, the largest organ and the first barrier of our body^[1], plays a vital role in protecting our body, but often becomes fragile when encountering different kinds of accidents, such as physical cuts and chemical reagent corrosion injury^[2,3]. In addition to the acute wounds caused by these accidents, chronic wounds such as diabetic foot ulcers (DFU), which are difficult to heal and cause serious physical damage, have become a major threat to human health and can lead to amputation and even death^[4,5]. As a temporary substitute, wound dressings provide durable protection in accelerating wound healing^[6]. Traditional wound dressings, such as bandages and gauze, have protective effects on wound surface, but often lack of ability to absorb tissue fluid and may cause secondary injuries due to adhesion on the wound surface^[7]. To solve these problems, membrane, sponge, rubber, hydrogel dressing, and other new dressings^[8-11] have been widely studied and used. Among the dressings described above, hydrogels can provide a moist environment to promote skin tissue regeneration and have structural characteristics similar to those of the extracellular matrix, as well as good slippery elasticity to avoid secondary injuries caused by lacerations^[12]. In addition, with the new modification and structural design, the hydrogel dressings are endowed with a variety of excellent properties, such as antibacterial, anti-inflammatory, and antioxidative properties, which are beneficial to the four stages of wound repair (hemostasis and coagulation, inflammation, proliferation, and remodeling)^[13].

Since hydrogel dressings are applied directly to the skin surface, it is essential to ensure that hydrogels are skin-friendly^[14], which involves the choice of hydrogel materials. Gelatin, a protein that partially hydrolyzed from collagen, has good biocompatibility and temperature sensitivity, and it is favored for its excellent viscoelasticity after solidification at low temperature (below 20°C)^[15]. Dou *et al.*^[16] introduced gelatin into poly (γ -glutamic acid) by physical crosslinking to improve the structural stability and cellular adhesion properties and form an excellent double-network bio-based wound dressing. Sodium alginate (SA) is a harmless natural polysaccharide extracted from brown algae^[17]. When a large number of high-valued metal cations such as Ca^{2+} , Mg^{2+} , and Cu^{2+} exist in the aqueous solution, they will be rapidly crosslinked with SA through replacing Na^+ to form gel networks^[18]. Hence, SA is widely used in hydrogel dressings due to mild reaction conditions^[19]. For example, Chen *et al.*^[20] used sodium alginate as a reducing agent and stabilizer to reduce Ag^+ into silver nanoparticles. Thereby, the nano-silver-loaded polyvinyl alcohol/sodium alginate wound dressings were prepared by using nano-silver as an antibacterial agent.

In order to prevent bacterial infestation, trauma dressings should have good antimicrobial activity^[21,22]. Although antibacterial agents have been widely developed and used, it has been a big problem to maintain excellent biocompatibility while having antibacterial properties^[22]. Some researchers have chosen to address this problem by adding antibiotics to the dressing. Antibiotics are efficient in destroying bacteria by inhibiting bacterial cell wall production or inhibiting protein and nucleic acid production within bacteria^[23,24], but the problems caused by antibiotics cannot be ignored, and some reports have mentioned that bacterial resistance and bacterial mutations are associated with heavy antibiotic use^[25,26]. Compared with antibiotics, biomacromolecular antimicrobial agents are safer and have sustained antimicrobial properties. Chitosan (CS) is the product of the deacetylation of chitin, a positively charged alkaline polysaccharide with low solubility in water^[27]. In order to improve its water solubility, quaternized groups are introduced to obtain quaternized chitosan (QCS). The cationic moieties of QCS are preferentially attracted to the negatively charged surfaces of bacteria, resulting in the disruption of bacterial membranes and efflux of internal material and ultimately in bacteria death^[28,29]. At the same time, its low biotoxicity and the addition of gelatin and SA as described above ensure that it will not cause damage to skin cells.

In damaged skin, inflammation-induced over-reactive oxygen species (ROS), including superoxide-free radicals and non-free radical hydrogen peroxides, alter or degrade extracellular matrix (ECM) proteins, destroy skin fibroblasts, and reduce keratinocyte function^[30,31]. Hydrogels loaded with free radical scavenging drugs have been shown to significantly improve the wound healing process in patients, avoiding oxidative damage^[32,33]. However, gelatin, SA, and QCS materials selected above have no antioxidant properties. Fortunately, the antioxidant capacity of hydrogels can be improved by grafting dopamine. As a neurotransmitter secreted by human body, dopamine has good biocompatibility and a large amount of catechol structure, which makes it an excellent free radical eliminator^[34,35].

Due to the accident of wounds, the randomness of the size and location of wounds, the dressing could not adapt to the changes of wounds^[36,37]. In order to fulfill different requirement of patients, 3D printing technology can be introduced to prepare hydrogel dressings according to their wound conditions. Moreover, the simple printing principle, cheap bioink material, and stable printing equipment make extrusion-based 3D printing conducive to the mass production of wound dressings^[38]. In addition, further research on 3D printing technology can pave the way for the emerging 4D printing technology and

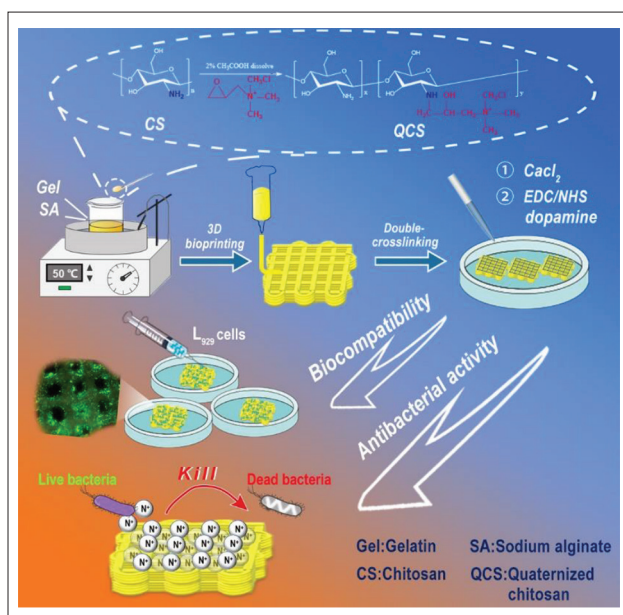


Figure 1. Schematic diagram of experimental process. The hydrogel was printed by an extrusion bioprinting technology with a bioink composed of gelatin, quaternized chitosan, sodium alginate, and grafting dopamine by EDC/NHS. The results showed that the hydrogel exhibited effective antioxidation ability, efficient hemocompatibility, high biocompatibility, and excellent antibacterial activity, suggested that it has a considerable potential to be applied in wound healing.

prepare intelligent biological hydrogel scaffolds for clinical application^[39]. Using 3D printing to prepare hydrogel dressings to speed up wound healing has many advantages over common hydrogel dressings^[40,41]. It is highly flexible where the size and shape of 3D printing dressings can be customized. Through 3D printing technology, the hydrogel dressing with suitable pores was designed with good air permeability, so as to avoid the formation of an anaerobic environment in the wound, which promotes the growth and propagation of anaerobic bacteria and causes the wound tissue hypoxia^[42]. Last, the 3D-printed dressings can quickly absorb exuded tissue fluid and provide a moist environment while facilitating drug release for wound healing^[43-45].

In this study, we aimed to fabricate a hydrogel dressing with effective antioxidation, excellent antibacterial activity and ideal biocompatibility (Figure 1). First, QCS is synthesized by CS grafting quaternary ammonium group. To enhance the printability and biocompatibility, the corresponding proportion of Gel and SA were mixed with QCS in the bioink (GAQ). The Gel/SA/QCS (GAQ) scaffold was fabricated by the extrusion 3D bioprinting, following ionic crosslinking with CaCl_2 . Then the Gel/SA/DA/QCS (GADQ) hydrogel was prepared by DA grafting onto the bioprinted GAQ scaffold with EDC/NHS crosslinking. We attempted to investigate the antioxidation, antibacterial

property, and biocompatible performance of the resulting double-crosslinked GADQ hydrogel dressings as potential medical applications for wound treatment.

2. Materials and methods

2.1. Materials

Chitosan (90% degree of deacetylation, and average molecular weight of 2×10^5 g/mol), gelatin (gel strength 240 g Bloom), sodium alginate (viscosity: 200–500 mPa·s), 2,3-epoxypropyltrimethylammonium chloride (GTMAC), 3-(3-Dimethylaminopropyl)-1-ethylcarbodiimide hydrochloride (EDC), dopamine, and N-hydroxysuccinimide (NHS) were provided by Adamas-beta® (Shanghai Titan Scientific Co.). Anhydrous calcium chloride (purity 96%) was obtained from Shanghai Maclin Biochemical Technology Co., Ltd.

The L929 fibroblast cell line was supplied from Qingqi (Shanghai) Biotechnology Development Co., Ltd. Cell Counting Kit-8 (CCK8) was purchased from Beyotime Biotechnology Co., Ltd. (Shanghai, China). The bacteria strains of *Escherichia coli* (*E. coli*, CICC 10899) and *Staphylococcus aureus* (*S. aureus*, CICC 21601) were purchased from Industrial Culture Collection (Beijing, China). Beef extract, agar powder, and peptone were acquired from Shanghai Bio-way Technology Co., Ltd. All other reagents were of analytical grade, unless otherwise stated.

2.2. Synthesis and characterization of QCS

The QCS was successfully synthesized based on the optimization of previous studies^[46]. Briefly, 2 g CS was added to deionized water, and acetic acid was introduced to dissolve CS completely under the rapid stirring of the rotor. Six gram GTMAC was slowly mixed in solution and the additive was fully reacted under stirring at 55°C for 21 h. When finished, the solution was centrifuged twice in a centrifuge at 10,000 rpm for 10 min to remove the undissolved polymer. Pre-cooled ethanol/acetone solution (1:1 v/v) was added to centrifugal solution to precipitate QCS. After filtration, the resulting precipitation was placed in the oven for complete drying and stored at room temperature. The degree of substitution (DS) of the QCS was calculated by determining the content of Cl^- in QCS by titration^[46]. The chemical structures of QCS were studied by ^1H NMR spectroscopy (Bruker 600MHz, Swiss) and Fourier transform infrared (FTIR) spectroscopy (BRUKER, USA).

2.3. Preparation of the Gel/Alg/QCS (GAQ) hybrid bioinks

A beaker filled with 40 mL ultrapure water was placed on a magnetic stirrer at 100 rpm. Subsequently, 2.4 g gelatin was added, followed by 0.6 g SA. While the mixture was being stirred until complete dissolved, different mass fractions

(0%, 0.5%, 1.0%, 1.5%w/v) of QCS were introduced into the solution. The selection of the maximum concentration of QCS is described in the section S1 of the Supplementary File. The samples with different m_{QCS} were named GAQ0%, GAQ0.5%, GAQ1.0%, and GAQ1.5%, respectively, where “G” stands for gelatin, “A” stands for SA, and “Q” stands for QCS.

2.4. Rheological properties of GAQ bioinks

Characteristics of rheology of Gel/Alg/QCS (GAQ) bioinks with gradient rate were tested to evaluate their printability. The parallel-plate rotational rheometer MCR 302 was used to test the temperature sensitivity, shear viscosity, and viscoelasticity of the inks. For the temperature sensitivity test, the temperature range was set as 10°C–40°C, the shear strain was 1%, and the frequency was 1 Hz. For shear viscosity test, the shear rate ranged from 0.01 to 1000 1/s. For viscoelastic test, the shear strain was set at 1%, and the angular frequency range was set at 0.01–100 rad/s.

2.5 Fabrication of the GADQ 3D hydrogels

The bioprinter (Bio-Architect, Regenovo Biotechnology Co., Ltd.) was controlled at a speed of 10 mm/s and an extrusion pressure of 0.21 MPa, Operating with a 24G (0.31 mm) nozzle. The temperature of the printer nozzle was controlled between 22°C and 25°C, and the platform temperature was maintained at 8°C through the water cooler. The printing model was set as 30 mm × 10 mm × 2 mm cuboid, and the filling distance was 0.8 mm.

The 3D-printed hydrogel scaffolds were immersed in a 50 mmol/L EDC/NHS and 2%(w/v) CaCl₂ crosslinking agent solution, and 0.2% (W/V) dopamine was added onto the crosslinked hydrogel network for 4 h. The hydrogels were washed with deionized water to remove surface EDC/NHS following freeze-drying, and then stored for later use.

2.6. Mechanical properties assay for the GADQ hydrogels

The tensile properties of 3D-printed hydrogel scaffolds were evaluated by a dynamic mechanics analyzer (Q800TA, USA). The samples (30 mm × 10 mm × 2 mm) were fixed in the drawing fixture. The drawing machine increased the tension with a speed of 1 N/min until the samples were fractured. The stress(σ) and strain(ϵ) values were obtained by the analyzer. The formula of tensile modulus is as follows:

$$E = \sigma/\epsilon \quad (\text{I})$$

The compression test is described in section S5 of the Supplementary File.

2.7. Swelling capacity and degradation test of the GADQ hydrogels

The swelling properties of hydrogels were determined by gravimetric analysis. The degradation test was described

in section S2 of the Supplementary File. The lyophilized hydrogels (GADQ0%, GADQ0.5%, GADQ1.0%, and GADQ1.5%) were weighed as W_0 . After soaking for a specific time in phosphate-buffered saline (PBS, 20 mL) at 25°C, the excess water on the surface of the hydrogels was wiped with filter paper and weighed as W_f . The swelling ratio was calculated by the following formula^[15]:

$$\text{Swelling ratio (\%)} = \frac{W_f - W_0}{W_0} \times 100\% \quad (\text{II})$$

2.8. Antioxidant capacity of the GADQ hydrogels

The antioxidant activity was evaluated by scavenging ability of DPPH-free radicals. Four same size (10 mm × 10 mm × 2 mm) samples (GADQ0%, GADQ0.5%, GADQ1.0%, and GADQ1.5%) were soaked in centrifuge tubes containing 3 mL DPPH (0.1 mmol/L) absolute ethanol solution, respectively, following incubation in a shaker with a speed of 200 rpm at 25°C for 15 min. UV spectrophotometer (UV-2600, Japan) was used to measure their absorbance value at 517 nm. The experimental groups were set as A_s , and the blank control group containing only DPPH was set as A_0 . The elimination ratio of DPPH can be calculated as follows^[47]:

$$\text{Antioxidant ability (\%)} = \left(1 - \frac{A_s}{A_0}\right) \times 100\% \quad (\text{III})$$

2.9. Hemolysis test of the GADQ hydrogels

The collected fresh rat blood was centrifuged at 1000 rpm for 10 min, and diluted to 2 v/v% with normal saline. Then, the diluted blood (5 mL) was co-cultured with these four hydrogels (size 10 mm × 10 mm × 2 mm) for 1 h at 37°C, respectively. One hour later, hydrogels were removed with tweezers, and blood suspension was centrifuged at 1500 rpm for 15 min. The absorbance of the supernatants was read at 540 nm by a UV spectrometer. The group added with 0.1% Triton X-100 was set as the positive control and the one added with regular saline was assigned as the negative control. The formula of hydrogel hemolysis ratio is as follows:

$$\text{Hemolysis (\%)} = \left[\frac{A_p - A_b}{A_t - A_b}\right] \times 100\% \quad (\text{IV})$$

where A_p represents the absorbance value of samples, A_t is the absorbance value of the Triton X-100 positive control, and A_b is the absorbance value of normal saline.

2.10. Antibacterial activity of the GADQ hydrogel

The GADQ hydrogel antibacterial activity was tested by the coating plate method and the determination method of bacterial concentration is described in section S4 of the Supplementary File^[48]. About 10⁵ CFU/mL of *E. coli* and *S. aureus* suspension (40 μ L) were evenly mixed into

sterilized Luria–Bertani broth (LB) medium (10 mL), respectively. The sterilized hydrogel (200 mg) was added to the culture medium injected with bacteria described above and incubated in a shaker with 100 rpm at 37°C for 24 h. The group without hydrogel was set as the positive control, and the group inoculated with no bacteria was set as the negative control. Then, 20- μ L bacterial suspension was evenly coated on the Nutrient Agar (NA) plates after diluting to a particular gradient, and cultured in an incubator at 37°C for 24 h. Finally, the colony forming units (CFU) in each plate was counted. The CFU in positive control group was set as P_0 , and the CFU in experimental group was set as P_s . The antibacterial activity of the hydrogels can be calculated with the formula as follows:

$$\text{Antibacterial activity (\%)} = \left(1 - \frac{P_s}{P_0}\right) \times 100\% \quad (\text{V})$$

2.11. *In vitro* biocompatibility test of the GADQ hydrogels

2.11.1. Cell culture and sterile inoculation of cells on scaffolds

The GADQ hydrogels were cut into the same size of 10 mm \times 10 mm \times 2 mm and placed into the 24-well plate, following sterilization in 75% ethanol and irradiation with UV light for 8 h. The hydrogels were immersed three times in sterile buffer solution to remove the remaining alcohol. L929 fibroblasts (1×10^5 cells/well) were transferred onto the hydrogels in 24-well plates, and cultured in complete medium containing 89% high glucose α -DMEM, 10% fetal bovine serum, and 1% antibiotics in the cell incubator set at 37°C and 5% carbon dioxide. One milliliter complete medium was added to each well after incubation of the 24-well plates in the incubator for 1 h to improve the adhesion ratio of cells onto the hydrogels, and the 24-well plates were then maintained in the culture incubator.

2.11.2. Live and dead staining of the GADQ hydrogels

Cell growth and proliferation on hydrogels can be determined by fluorescence colorimetry. At first, the cell-hydrogels complex to days 1, 4, and 7 were transferred to new 24-well plates. Then, 250 μ L triple-staining reagent, which was prepared by mixing 1 mL PBS with 5 μ L Hoechst, 2 μ L calcein, and 1 μ L propidium iodide (PI), was added to each well and incubated at 37°C for 30 min. The color development of the three stains of the cell-hydrogel was analyzed under a fluorescence microscope (IX70, Japan).

2.11.3. Scanning electron microscopy (SEM) for the GADQ hydrogels

After culturing for 1, 4, and 7 days, the cells were immobilized on the hydrogel with 2.5% glutaraldehyde. The cell-hydrogels were subjected to gradient dehydration

with 60%, 75%, 95%, and 100% ethanol solutions for 30 min, respectively. The samples were sputter-coated with gold, and the growth of cells on the scaffolds were observed using scanning electron microscope.

2.11.4. Cytotoxicity test for the GADQ hydrogels

The relative viability of cells on GADQ hydrogels was detected by CCK-8 test. The cell-hydrogels cultured for 1, 3, 5, and 7 days were immersed in 300 μ L of CCK-8 reagent in each well, and incubated at 37°C for 2.5 h. After uniform mixing with a pipette, 100 μ L of the mixture from each group was taken for absorbance determination at 450 nm by the microplate reader^[49]. The control group was set as GADQ0% on day 1. The formula is as follows:

$$\text{Cell relative viability (\%)} = \frac{\text{OD}_{\text{Sample}}}{\text{OD}_{\text{Control}}} \times 100\% \quad (\text{VI})$$

3. Results and discussions

3.1. Preparation and detections of QCS and hybrid bioinks

The titration of QCS with AgNO_3 is shown in Figure 2a, and the calculated substitution degree of QCS was 63.31%. The FT-IR of CS, QCS and GADQ is shown in Figure 2b. The peak of CS, QCS, and GADQ1.5% at 1590 cm^{-1} was attributed to N-H bending vibration. Similar peaks of N-H bending vibration from gelatin and dopamine can be found at 1630 cm^{-1} in GADQ0% and 1641 cm^{-1} in GADQ1.5%. According to the literature^[50], the peak at 1385 cm^{-1} was attributed to the bending vibration of methyl left by incomplete deacetylation of chitosan, which was not present in GADQ0%. The spectra of QCS and GADQ1.5% had a distinct characteristic peak corresponding to the methyl bond of quaternary ammonium salt at 1453 cm^{-1} , while the spectra of CS and GADQ0% did not have this peak. At the same time, the chemical structure of CS and QCS was confirmed by ^1H NMR, as shown in Figure 2c and d. The signal range of H1–H6 proton was 2.71–4.39 ppm, and the additional peaks at 1.83 (H-c), 2.06 (H-a), and 3.165 ppm (H-d) were from the modified quaternary ammonium group on CS^[51]. Significantly, the highest signal at 3.165 ppm was provided by the proton signal of three methyl groups on the quaternary ammonium group ($-\text{N}^+(\text{CH}_3)_3$). The above studies effectively proved the synthesis of QCS.

3.2. Rheological properties of the GAQ bioinks

The temperature sensitivity of bioink is shown in Figure 3a and b. Due to the storage modulus and composite viscosity increased as temperature decreased, gelation appeared in the fluidic hydrogel. This sudden fluid-gel transition was called gel point and the corresponding temperature was known as minimum gel temperature. Figure 3c shows the storage

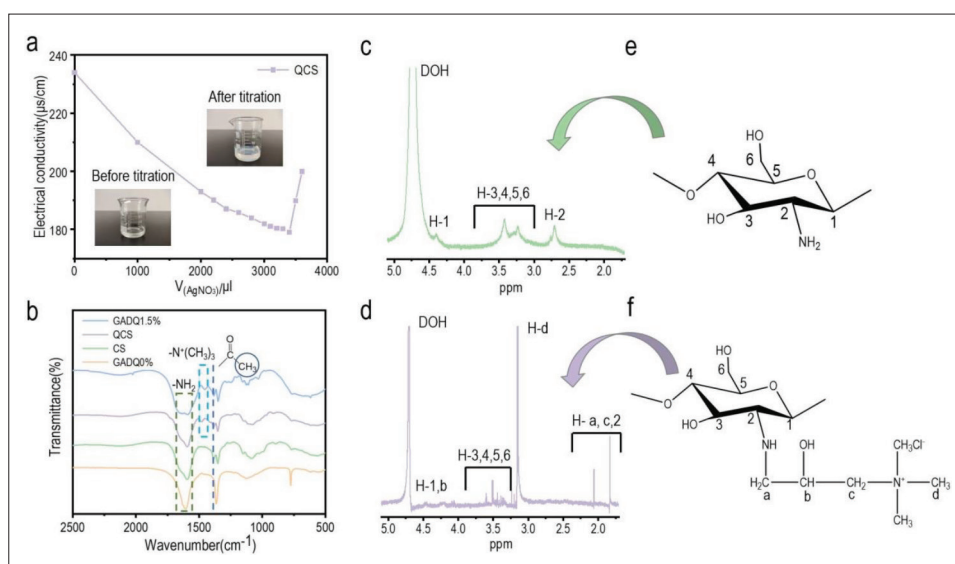


Figure 2. Preparation of QCS and inks. (a) Titration of chloride ions in QCS by AgNO₃. (b) FTIR spectra of CS, QCS, GADQ0%, and GADQ1.5%. (c and d) 1H NMR spectra of CS and QCS. (e and f) CS and QCS structural formulae corresponding to 1H NMR spectra peaks.

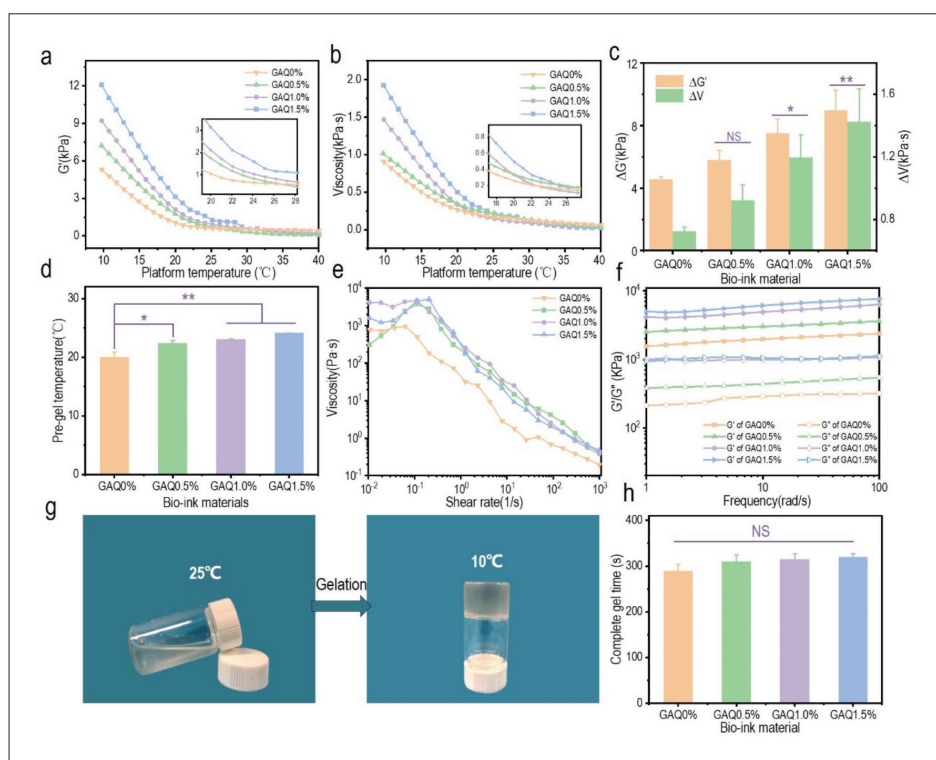


Figure 3. The rheological properties of the GAQ inks. The (a) storage modulus (G') and (b) composite viscosity (V) of the inks with the change of temperature. Inserted picture: partial curves from 28°C to 19°C. (c) Characterization of inks storage modulus deviation value ($\Delta G'$) and viscosity deviation value (ΔV) at 25°C and 10°C. (d) Pre-gel temperature of the bioinks. (e) Viscosity of the bioinks versus shear rate from 0.01 to 1000 s⁻¹ at 25°C. (f) Dynamic storage modulus (G') and loss modulus (G'') of the inks at varying frequency of 1–100 rad/s at 25°C with 1% constant shear strain. (g) Gelation of the GAQ ink from 25°C to 10°C. (h) Characterization of complete gel time of the four inks from 25°C to 10°C. Data are expressed as mean \pm SD. NS: $p > 0.05$; * $p < 0.05$ and ** $p < 0.01$.

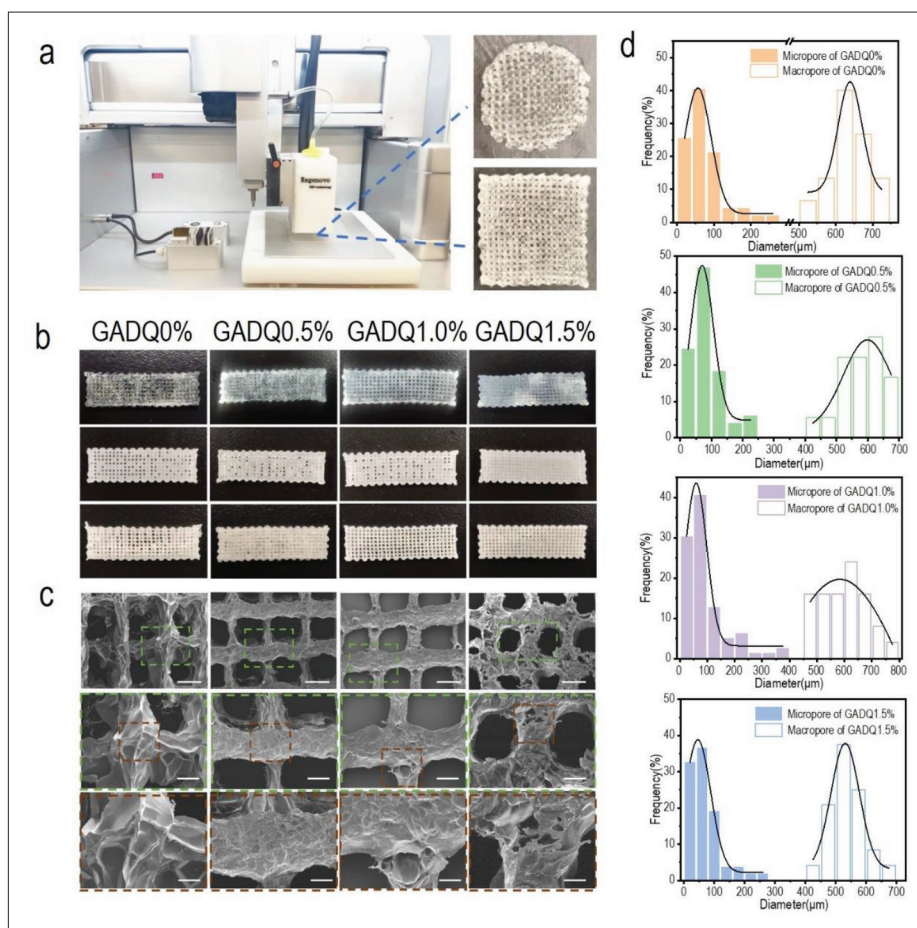


Figure 4. Morphology and structure characterization of the GADQ hydrogels. (a) 3D bioprinter and 3D-printed round and square hydrogels. (b) The optical images of hydrogel after 3D printing in this experiment. The top row is the hydrogels without crosslinking; the middle is the hydrogels after crosslinking; and the bottom is the freeze-dried hydrogels after crosslinking. (c) SEM images of the freeze-dried GADQ hydrogels. Scale bar: 500 μm in the top; 200 μm in the middle; 100 μm in the bottom. (d) Pore diameter distributions of the hydrogels.

modulus deviation value ($\Delta G'$) and composite viscosity deviation value (ΔV) of the four hydrogels between 10°C and 25°C, which illustrated the temperature sensitivity of the bioinks. GAQ1.5% had the highest $\Delta G'$ and ΔV , which was theoretically the best to print. The minimum gel temperature is shown in Figure 3d. The results indicated that GAQ1.5% has the best temperature sensitivity, and the critical gel temperature was 24.14°C, which was similar to the room temperature. Figure 3e presents the shear viscosity analysis of the inks. When the shear rate exceeded 0.1 s⁻¹, the viscosity of the inks decreased significantly as shear rate increased. When the shear rate reached 1000 s⁻¹, the viscosity of all the four inks was less than 1 Pa·s, indicating that inks can be easily extruded from the needles with high shear force during 3D printing^[52]. The viscoelasticity of bioinks is shown in Figure 3f. Our results showed that all the inks have a higher G' (storage modulus) than G'' (loss modulus) at 25°C, indicating that hydrogels did not liquefy at room temperature. Among them, GAQ1.5% had high elasticity and relatively low

viscosity force, which would perform the best printability. Figure 3g shows the gelation of the GAQ bioink from 25°C to 10°C, the complete gel time of four inks decreased from 25°C to 10°C, as shown in Figure 3h. Among the four inks, the complete gel time of GAQ1.5% was the longest, but there was no significant difference from other concentrations. All four inks could be used for 3D bioprinting, which revealed the advantages of introducing QCS.

3.3. Morphology characterization of the GADQ hydrogels

The 3D-printed round and square hydrogel dressings are shown in Figure 4a. In this experiment, a 30 mm × 10 mm × 2 mm cuboid model was used for fabricating hydrogel dressing by 3D printing. The optical images of the printed hydrogels are shown in Figure 4b. With the increase of QCS mass ratio, the pore structure of the hydrogels became more compact, and the appearance of GADQ1.5% hydrogel was more regular when compared to others. SEM of the

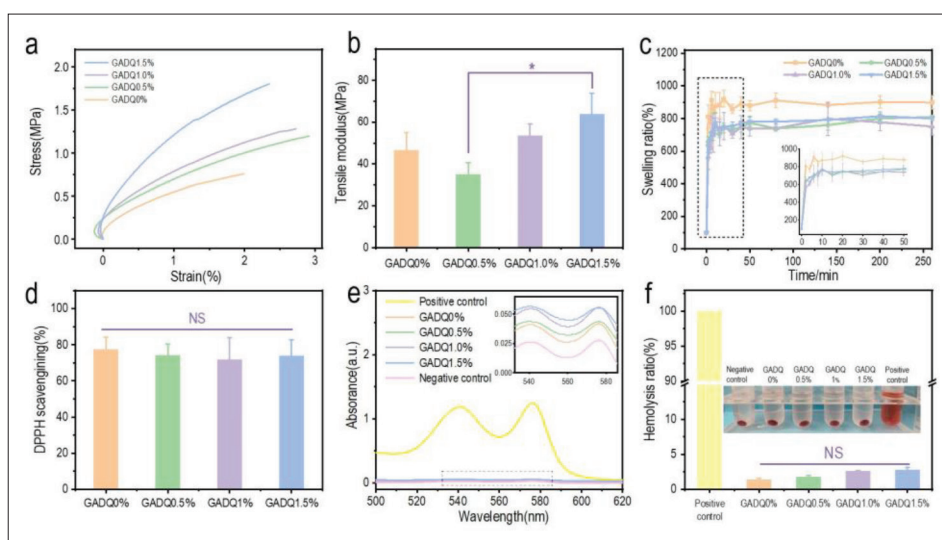


Figure 5. Characterization of GADQ hydrogel properties. (a) Stress–strain curves of the hydrogels at a tension rate of 1 N/min. (b) Tensile modulus of the hydrogels. (c) Swelling ratio of the hydrogels during 6 h in PBS (pH 7.4) at 25°C. (d) DPPH scavenging percentage by the hydrogels. (e) The hemolysis ratios of the hydrogels were measured by UV spectrum with a wavelength range of 500–620 nm. (f) The quantitative hemolysis ratio of the hydrogels. Triton X-100 was set as the positive control and physiological saline was set as the negative control. Data are expressed as mean \pm SD (n = 3). NS: $p > 0.05$; * $p < 0.05$.

3D-printed hydrogels revealed a regular macroporous structure formed by the spacing parameter, as well as the formation of many interconnected micropores inside the hydrogel after lyophilization (Figure 4c). Analysis of pore distribution indicated that both micropore and macropore size of hydrogels displayed Gaussian distribution (Figure 4d). The macropore size distribution of these printed hydrogels was between 500 and 800 μm , providing sufficient space for cell growth and differentiation. The average macropore size of GADQ0% was 620 μm , while that of GADQ1.5% was 540 μm . This phenomenon showed that with the increase of QCS content, the crosslinking density of hydrogel also increased, but the pore size decreased. The interconnected micropores (mainly 0–200 μm) in the hydrogel were favorable for proliferation and migration of fibroblasts (10–15 μm). The large number of micropores also facilitated nutrient delivery and the elimination of cellular metabolic waste. Both macropores and micropores provided assurance for wound healing.

3.4. Mechanical properties, swelling capacity, and degradation of the GADQ hydrogels

Hydrogel dressings can easily be damaged by pulling forces during medical treatment. The mechanical property was evaluated by tensile tests and compression tests. As shown in Figure 5a, the curve slope of the hydrogels has no significant difference when the QCS concentration was lower than 1.5% (GADQ0.5% and GADQ1%), and the curve slope of GADQ1.5% was significantly increased compared to the others. Figure 5b shows that the tensile modulus of GADQ1.5% (63.85 ± 9.95 MPa) significantly increased to

GADQ0.5% (35.10 ± 5.49 MPa). In addition, according to the stress–strain curve, the stress of GADQ0.5% was only slightly higher than that of GADQ0%, but its strain value was twice higher than that of GADQ0%, which explained that the tensile modulus of GADQ0.5% is lower than that of GADQ0%. The hydrogel would be easily deformed and broken when the concentration of QCS was low (GADQ0.5%). The GADQ hydrogel compression analysis is described in section S6 of the Supplementary File. The compression stress strain curves and compression strength are shown in Figure S6.

With good swelling properties, hydrogel could effectively absorb tissue fluid exuded from the wound and adhere to the skin without causing damage to the skin. Figure 5c shows the swelling ratios of four hydrogels within 300 min. The four hydrogels reached swelling equilibrium at approximately 50 min (Figure 5c enlarged view). GADQ0% had the highest swelling ratio of 878%, while the remaining three hydrogels had similar swelling ratio of about 780%. This is because $-\text{NH}_2$ in QCS crossed in hydrogel networks, which made hydrogel firm and reduced the swelling rate. Fortunately, the swelling ratio did not decrease further as the concentration of QCS increased. It indicated that QCS would not affect the swelling ratio in a certain concentration range, and more importantly, it effectively avoids excessive swelling of hydrogel. Therefore, GADQ1.5% hydrogels could absorb excess tissue exudate while maintaining a wet environment during wound healing.

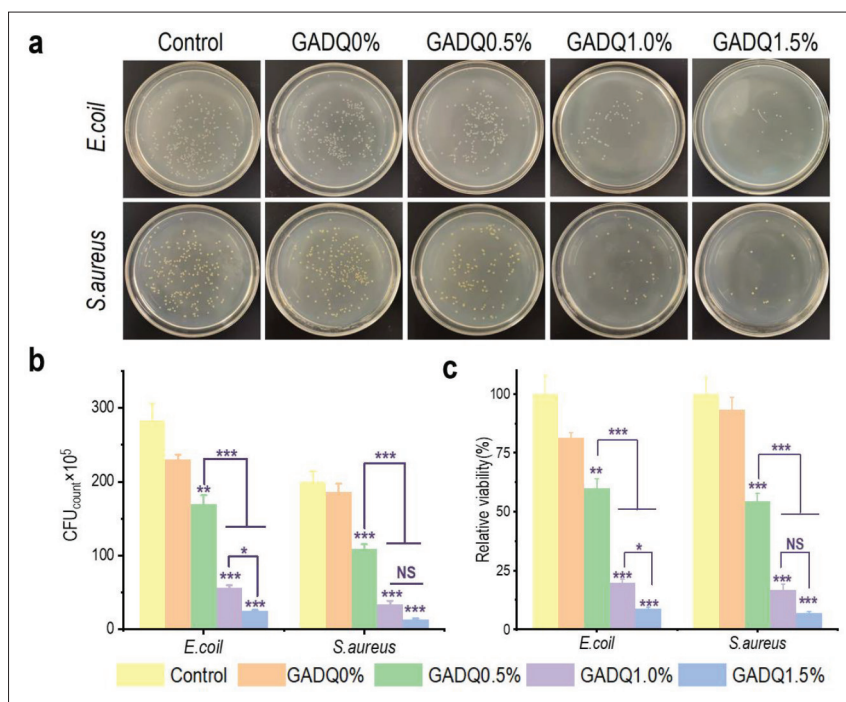


Figure 6. Antibacterial activity of the GADQ hydrogels. (a) Optical images of colony count of the hydrogels against *E. coli* and *S. aureus* (the incubation time is 24 h). (b) Corresponding statistical data of colonies of *E. coli* and *S. aureus* cultured with the GADQ hydrogels. (c) Relative activity of *E. coli* and *S. aureus* cultured with the scaffolds. Data are expressed as mean \pm SD. NS: $p > 0.05$; * $p < 0.05$, ** $p < 0.01$, *** $p < 0.001$. Note: the * above the column indicates the comparison of each group with control group.

GADQ hydrogel degradation analysis is described in section S3 of the Supplementary File. The change of degradation rate over time is shown in [Figure S2](#).

3.5. Antioxidant and hemolysis properties of the GADQ hydrogels

Large number of free radicals could be present at the wound site and would cause oxidative stress that leads to DNA breakage and enzyme inactivation, which will result in the extensive collateral damage to the surrounding skin wound sites and cause persistent ulcers^[53]. The application of free radical-scavenging hydrogels has been proven to accelerate wound repair. Therefore, dopamine containing polyphenol hydroxyl functional groups was introduced into the hydrogels through EDC/NHS crosslinking, and antioxidant activity were evaluated by detecting the scavenging efficiency of DPPH. As shown in [Figure 5d](#), the DPPH scavenging rate of the four hydrogels was more than 70%, indicating that increasing the content of QCS did not affect the antioxidant activity of hydrogels. Overall, the GADQ1.5% hydrogels with excellent antioxidant property are expected to be novel wound dressings.

As a medical dressing, hydrogels should have good blood compatibility and be friendly to blood cells. The UV spectrum of each supernatant after centrifugation is shown in [Figure 5e](#), which demonstrates that hemoglobin

shows prominent absorption peaks at 540 nm and 575 nm. Hence, the hemolysis ratio was measured by reading the absorbance of the supernatant at 540 nm. As shown in [Figure 5f](#), the hemolysis rate of hydrogels increased with the rise of QCS concentration. However, they did not reach the limit of 5%, and GADQ1.5% was the hydrogel manifesting the highest hemolysis (2.81%), with hemocompatibility similar to or better than that of hemostatic materials as previously reported^[54]. There is no significant difference when it was compared to GADQ0% hydrogel, indicating that the GADQ hydrogels prepared in this study have good blood compatibility.

3.6. Antibacterial properties of the GADQ hydrogels

Bacteria are found almost everywhere, but wound is too fragile to prevent bacterial invasion so good hydrogel dressings should be in place to provide protection against bacterial growth. [Figure 6a](#) and [b](#) show colony forming units (CFU) of *E. coli* and *S. aureus* cultured for 24 h with the hydrogels, reflecting CFU decrease with the increase of QCS concentration. According to the results shown in [Figure 6c](#), GADQ1.5% had the best antibacterial activity against *E. coli* and *S. aureus* of $91.06 \pm 0.44\%$ and $93.17 \pm 0.62\%$, respectively, when compared to GADQ0.5% ($40.04 \pm 4.09\%$, $45.5 \pm 3.19\%$) and GADQ1% ($80.16 \pm 1.38\%$, $83.17 \pm 2.46\%$). The results that GADQ hydrogel can kill *S.*

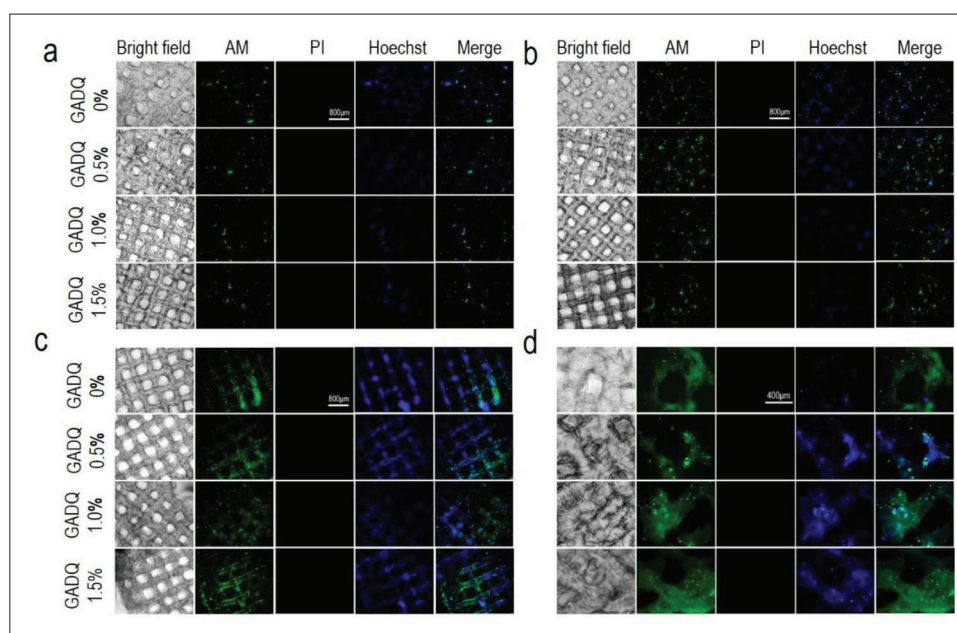


Figure 7. *In vitro* live-dead staining test. (a–c) The fluorescent staining of the cell-hydrogels at days 1, 4, and 7 (40× magnification). Scale bar: 800 μm. (d) The fluorescent staining of cell-hydrogels at day 7 (100× magnification). Scale bar: 400 μm.

aureus more effectively than *E. coli* were attributed to the fact that the cell wall of *S. aureus* is completely composed of peptidoglycan while *E. coli* is composed of peptidoglycan and an outer lipopolysaccharide layer, which acts as a barrier against macromolecules to some extent^[55,56]. The remarkable antibacterial performance of GADQ1.5% showed great potential in efficiently preventing wound infection.

3.7. Cytotoxicity assay of the GADQ hydrogel dressings

During wound healing process, in addition to preventing bacterial infection, wound dressings should also ensure the normal growth and activity of skin cells. The biocompatibility of GADQ hydrogel was evaluated by L929 fibroblasts. Figure 7a–d show the staining of cells on hydrogels. Different intensities of green fluorescence indicate the location and number of cells, as shown in Figure 7a–c. With the increase of culture days, we observed that the cells adhered onto and proliferated well on the pores of the four hydrogels using calcein-AM and Hoechst stainings. In these four hydrogels, the growth rate of fibroblasts on GADQ0% was the fastest. After cultured for 7 days as shown in Figure 7c, the cells proliferated and distributed on the outer and inner surface of the GADQ hydrogels, and the density of cells on hydrogels at day 7 significantly increased when compared to days 1 and 4.

Figure 8a shows the SEM images of L929 cells inoculated on four hydrogels on days 1, 4, and 7. Cell clusters began to integrate on the hydrogels on day 4. Due to the favorable sites for cell adhesion, synapses were initially formed and

adhered to each other to form cell aggregates in hydrogels. On day 7, the proliferation of cells on the hydrogels was more pronounced and showed good cell morphology. The results confirmed the fluorescence staining above. Moreover, the cell survival rate on the hydrogels was quantified by CCK-8 assay, with the results shown in Figure 8b. The cell survival ratio of GADQ0% on day 1 was set at 100% as the relative value to the other groups. The results displayed that there is no apparent difference between GADQ0.5%, GADQ1.0%, GADQ1.5%, and GADQ0% at days 1, 3, 5, and 7. Compared with GADQ0%, the hydrogels added with QCS may promote cell adhesion due to its good sliding elasticity, and its excellent mechanical support properties provide a more stable growth space. GADQ1.5% not only had good cell adhesion but also did not cause excessive damage to cells. As a result, GADQ1.5% was the potential hydrogel material with good biocompatibility.

4. Conclusion

In this work, the substitution degree of 63.31% QCS was synthesized, then Gel, SA, and QCS were configured to the inks with good rheology, and finally, the 3D hydrogels with good biocompatibility were fabricated using 3D printing. Among the GADQ hydrogels with different mass fractions of QCS, GADQ1.5% has the best tensile properties, appropriate swelling ratio, stable antioxidant performance (exceeding 70%), and good biocompatibility. More importantly, it had the best antibacterial activity against *E. coli* and *S. aureus* of $91.06 \pm 0.44\%$ and $93.17 \pm 0.62\%$, respectively. At the same time, GADQ1.5% showed

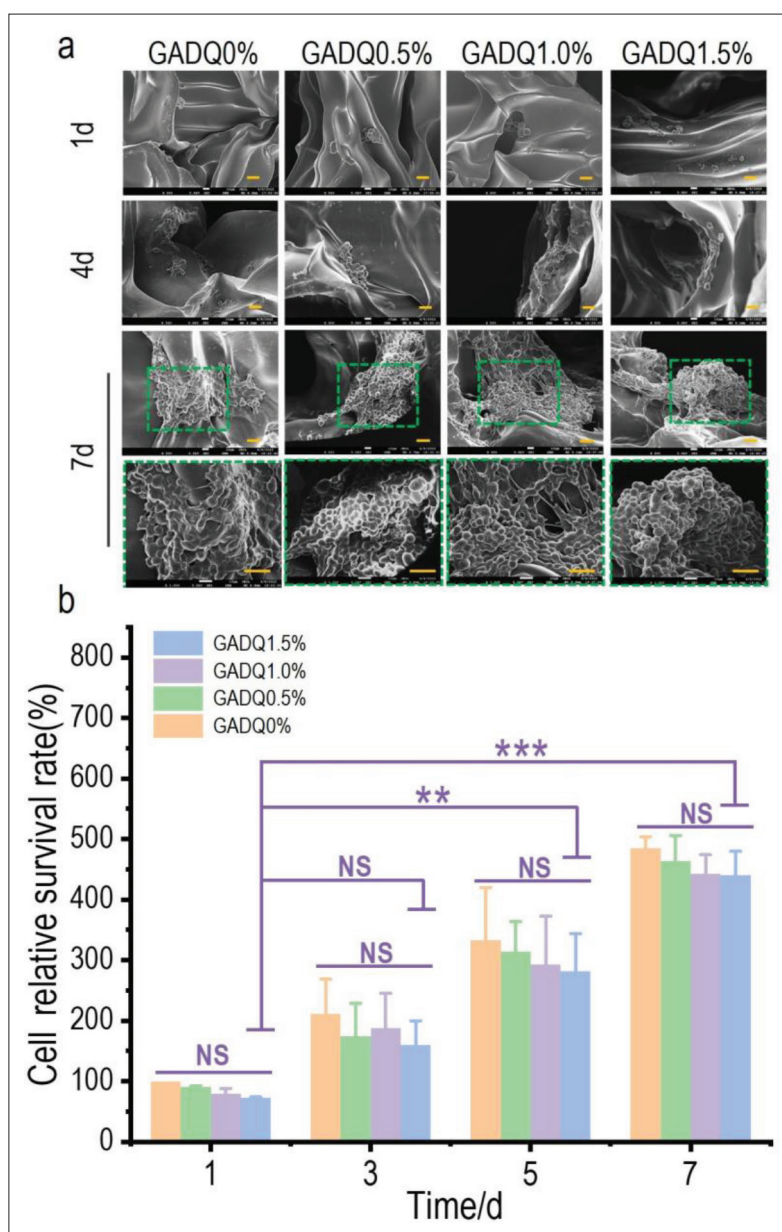


Figure 8. The morphological observation of L929 fibroblasts on the hydrogels by SEM and cytotoxicity test of the hydrogels. (a) The SEM images of fibroblasts cultured on the hydrogels for 1, 4, and 7 days (500× magnification, scale bar: 20 μm) and the enlarged images of fibroblasts for 7 days (1000× magnification, scale bar: 20 μm). (b) Cell survival ratio on the hydrogels tested by CCK-8. Data are expressed as mean ± SD. NS: $p > 0.05$; * $p < 0.05$, ** $p < 0.01$, *** $p < 0.001$.

superior biocompatibility based on live and dead staining test, SEM images and CCK-8 assay. The strategy of combining the advantages of 3D printing and several biocompatible materials in this study provided an inspiration for the design of multifunctional dressing for wound healing.

Acknowledgments

None.

Funding

This work was supported by the National Natural Science Foundation of China (31670978/32000977), the Fok Ying Tung Education Foundation (132027), the State Key Laboratory of Fine Chemicals (KF1111), and the Fundamental Research Funds for the Central Universities (DUT20ZD206/ DUT21YG113/DUT22YG213) and Natural Science Foundation of Shandong Province (ZR2020QH188).

Conflict of interest

The authors declare no conflicts of interest.

Author contributions

Conceptualization: Kedong Song, Yi Nie, Yueqi Lu

Data curation: Yueqi Lu, Jie Xu, Huan Fang

Formal analysis: Yueqi Lu, Jie Xu, Ya Su, Huan Fang, Jiaqi Liu, Siyao Lv

Investigation: Yueqi Lu, Jie Xu, Ya Su

Methodology: Kedong Song, Yueqi Lu, Jie Xu, Yi Nie

Project administration: Kedong Song

Supervision: Kedong Song, Yi Nie, Bo Pan, Wenfang Li

Validation: Kedong Song, Yi Nie, Bo Pan, Wenfang Li

Visualization: Yueqi Lu, Jie Xu, Huan Fang, Kedong Song

Writing – original draft: Yueqi Lu, Jie Xu, Jiaqi Liu, Siyao Lv, Yuen Yee Cheng

Writing – review & editing: Kedong Song, Yuen Yee Cheng, Yueqi Lu, Jie Xu, Jiaqi Liu

Ethics approval and consent to participate

The experiments described in this work were approved by the Biological and Medical Ethics Committee, Dalian University of Technology (DLUTSCE20221027-01).

Consent for publication

Not applicable.

Availability of data

Not applicable.

References

1. Zhao X, Wu H, Guo B, *et al.*, 2017, Antibacterial anti-oxidant electroactive injectable hydrogel as self-healing wound dressing with hemostasis and adhesiveness for cutaneous wound healing. *Biomaterials*, 122:34–47.
<https://doi.org/10.1016/j.biomaterials.2017.01.011>
2. Wang X, Qi J, Zhang W, *et al.*, 2021, 3D-printed antioxidant antibacterial carboxymethyl cellulose/epsilon-polylysine hydrogel promoted skin wound repair. *Int J Biol Macromol*, 187:91–104.
<https://doi.org/10.1016/j.ijbiomac.2021.07.115>
3. Feng Z, Su Q, Zhang C, *et al.*, 2020, Bioinspired nanofibrous glycopeptide hydrogel dressing for accelerating wound healing: A cytokine-free, M2-type macrophage polarization approach. *Adv Funct Mater*, 30(52):2006454.
<https://doi.org/10.1002/adfm.202006454>
4. Liu G, Zhou Y, Xu Z, *et al.*, 2022, Janus hydrogel with dual antibacterial and angiogenesis functions for enhanced diabetic wound healing. *Chin Chem Lett*.
<https://doi.org/10.1016/j.ccllet.2022.07.048>
5. Xian C, Zhang Z, You X, *et al.*, 2022, Nanosized fat emulsion injection modulating local microenvironment promotes angiogenesis in chronic wound healing. *Adv Funct Mater*, 32(32):2202410.
<https://doi.org/10.1002/adfm.202202410>
6. Zakerikhoob M, Abbasi S, Yousefi G, *et al.*, 2021, Curcumin-incorporated crosslinked sodium alginate-g-poly (N-isopropyl acrylamide) thermo-responsive hydrogel as an in-situ forming injectable dressing for wound healing: In vitro characterization and in vivo evaluation. *Carbohydr Polym*, 271:118434.
<https://doi.org/10.1016/j.carbpol.2021.118434>
7. Li M, Liang Y, He J, *et al.*, 2020, Two-pronged strategy of biomechanically active and biochemically multifunctional hydrogel wound dressing to accelerate wound closure and wound healing. *Chem Mater*, 32(23):9937–9953.
<https://doi.org/10.1021/acs.chemmater.0c02823>
8. Tran PL, Hamood AN, de Souza A, *et al.*, 2015, A study on the ability of quaternary ammonium groups attached to a polyurethane foam wound dressing to inhibit bacterial attachment and biofilm formation. *Wound Repair Regen*, 23(1):74–81.
<https://doi.org/10.1111/wrr.12244>
9. Li J, Zhai D, Lv F, *et al.*, 2016, Preparation of copper-containing bioactive glass/eggshell membrane nanocomposites for improving angiogenesis, antibacterial activity and wound healing. *Acta Biomater*, 36:254–266.
<https://doi.org/10.1016/j.actbio.2016.03.011>
10. Fan Z, Liu B, Wang J, *et al.*, 2014, A novel wound dressing based on Ag/graphene polymer hydrogel: Effectively kill bacteria and accelerate wound healing. *Adv Funct Mater*, 24(25):3933–3943.
<https://doi.org/10.1002/adfm.201304202>
11. Rieger KA, Birch NP, Schiffman JD, 2013, Designing electrospun nanofiber mats to promote wound healing—A review. *J Mater Chem B*, 1(36):4531–4541.
<http://doi.org/10.1039/c3tb20795a>
12. Shu W, Wang Y, Zhang X, *et al.*, 2021, Functional hydrogel dressings for treatment of burn wounds. *Front Bioeng Biotech*, 9:788461.
<https://doi.org/10.3389/fbioe.2021.788461>
13. Wang L, Zhou M, Xu T, *et al.*, 2022, Multifunctional hydrogel as wound dressing for intelligent wound monitoring. *Chem Eng J*, 433:134625.
<https://doi.org/10.1016/j.cej.2022.134625>

14. Liu SQ, Zheng RM, Chen S, *et al.*, 2018, A compliant, self-adhesive and self-healing wearable hydrogel as epidermal strain sensor. *J Mater Chem C*, 6(15):4183–4190.
<https://doi.org/10.1039/c8tc00157j>
15. Sun M, Sun X, Wang Z, *et al.*, 2018, Synthesis and properties of gelatin methacryloyl (GelMA) hydrogels and their recent applications in load-bearing tissue. *Polymers*, 10(11):1290.
<https://doi.org/10.3390/polym10111290>
16. Dou C, Li Z, Luo Y, *et al.*, 2022, Bio-based poly (gamma-glutamic acid)-gelatin double-network hydrogel with high strength for wound healing. *Int J Biol Macromol*, 202:438–452.
<https://doi.org/10.1016/j.ijbiomac.2022.01.057>
17. Gomez CG, Rinaudo M, Villar MA, 2007, Oxidation of sodium alginate and characterization of the oxidized derivatives. *Carbohydr Polym*, 67(3):296–304.
<https://doi.org/10.1016/j.carbpol.2006.05.025>
18. Abasalizadeh F, Moghaddam SV, Alizadeh E, *et al.*, 2020, Alginate-based hydrogels as drug delivery vehicles in cancer treatment and their applications in wound dressing and 3D bioprinting. *J Biol Eng*, 14(1):17.
<https://doi.org/10.1186/s13036-020-0227-7>
19. Shao Y, Wu C, Wu T, *et al.*, 2018, Green synthesis of sodium alginate-silver nanoparticles and their antibacterial activity. *Int J Biol Macromol*, 111:1281–1292.
<https://doi.org/10.1016/j.ijbiomac.2018.01.012>
20. Chen K, Wang F, Liu S, *et al.*, 2020, In situ reduction of silver nanoparticles by sodium alginate to obtain silver-loaded composite wound dressing with enhanced mechanical and antimicrobial property. *Int J Biol Macromol*, 148:501–509.
<https://doi.org/10.1016/j.ijbiomac.2020.01.156>
21. Lu B, Han X, Zou D, *et al.*, 2022, Catechol-chitosan/polyacrylamide hydrogel wound dressing for regulating local inflammation. *Mater Today Biol*, 16:100392.
<https://doi.org/10.1016/j.mtbio.2022.100392>
22. Zou F, Wang Y, Tang T, *et al.*, 2023, Synergistic strategy constructed hydrogel-aerogel biphasic gel (HAB-gel) with self-negative-pressure exudate absorption, M2 macrophage-polarized and antibacterial for chronic wound treatment. *Chem Eng J*, 451:138952.
<https://doi.org/10.1016/j.cej.2022.138952>
23. Zhu L, Chen L, 2022, Facile design and development of nano-clustery graphene-based macromolecular protein hydrogel loaded with ciprofloxacin to antibacterial improvement for the treatment of burn wound injury. *Polym Bull*, 79(9): 7953–7968.
<https://doi.org/10.1007/s00289-021-03875-8>
24. Allen R, Waclaw B, 2016, Antibiotic resistance: A physicist's view. *Phys Biol*, 13(4):045001.
<https://doi.org/10.1088/1478-3975/13/4/045001>
25. Jiang S, Deng J, Jin Y, *et al.*, 2023, Breathable, antifreezing, mechanically skin-like hydrogel textile wound dressings with dual antibacterial mechanisms. *Bioact Mater*, 21: 313–323.
<https://doi.org/10.1016/j.bioactmat.2022.08.014>
26. Pang Q, Lou D, Li S, *et al.*, 2020, Smart flexible electronics-integrated wound dressing for real-time monitoring and on-demand treatment of infected wounds. *Adv Sci*, 7(6):1902673.
<https://doi.org/10.1002/advs.201902673>
27. Jayakumar R, Prabakaran M, Nair SV, *et al.*, 2010, Novel chitin and chitosan nanofibers in biomedical applications. *Biotechnol Adv*, 28(1):142–150.
<https://doi.org/10.1016/j.biotechadv.2009.11.001>
28. Wang X, Xu P, Yao Z, *et al.*, 2019, Preparation of antimicrobial hyaluronic acid/quaternized chitosan hydrogels for the promotion of seawater-immersion wound healing. *Front Bioeng Biotech*, 7:360.
<https://doi.org/10.3389/fbioe.2019.00360>
29. Matica MA, Aachmann FL, Tondervik A, *et al.*, 2019, Chitosan as a wound dressing starting material: Antimicrobial properties and mode of action. *Int J Mol Sci*, 20(23):5889.
<https://doi.org/10.3390/ijms20235889>
30. Liang Y, Zhao X, Hu T, *et al.*, 2019, Mussel-inspired, antibacterial, conductive, antioxidant, injectable composite hydrogel wound dressing to promote the regeneration of infected skin. *J Colloid Interface Sci*, 556:514–528.
<https://doi.org/10.1016/j.jcis.2019.08.083>
31. Loo AEK, Wong YT, Ho R, *et al.*, 2012, Effects of hydrogen peroxide on wound healing in mice in relation to oxidative damage. *PLoS One*, 7(11):e49215.
<https://doi.org/10.1371/journal.pone.0049215>
32. Tang P, Han L, Li P, *et al.*, 2019, Mussel-inspired electroactive and antioxidative scaffolds with incorporation of polydopamine-reduced graphene oxide for enhancing skin wound healing. *ACS Appl Mater Interfaces*, 11(8):7703–7714.
<https://doi.org/10.1021/acsami.8b18931>
33. Ou Q, Zhang S, Fu C, *et al.*, 2021, More natural more better: Triple natural anti-oxidant puerarin/ferulic acid/polydopamine incorporated hydrogel for wound healing. *J Nanobiotechnol*, 19(1):237.
<https://doi.org/10.1186/s12951-021-00973-7>

34. Neto AI, Cibrao AC, Correia CR, *et al.*, 2014, Nanostructured polymeric coatings based on chitosan and dopamine-modified hyaluronic acid for biomedical applications. *Small*, 10(12):2459–2469.
<https://doi.org/10.1002/sml.201303568>
35. Hong S, Yang K, Kang B, *et al.*, 2013, Hyaluronic acid catechol: A biopolymer exhibiting a pH-dependent adhesive or cohesive property for human neural stem cell engineering. *Adv Funct Mater*, 23(14):1774–1780.
<https://doi.org/10.1002/adfm.201202365>
36. Leppiniemi J, Lahtinen P, Pajanen A, *et al.*, 2017, 3D-printable bioactivated nanocellulose-alginate hydrogels. *ACS Appl Mater Interfaces*, 9(26):21959–21970.
<https://doi.org/10.1021/acsami.7b02756>
37. Teoh JH, Mozhi A, Sunil V, *et al.*, 2021, 3D printing personalized, photocrosslinkable hydrogel wound dressings for the treatment of thermal burns. *Adv Funct Mater*, 31(48):2105932.
<https://doi.org/10.1002/adfm.202105932>
38. Guo Y, Huang J, Fang Y, *et al.*, 2022, 1D, 2D, and 3D scaffolds promoting angiogenesis for enhanced wound healing. *Chem Eng J*, 437:134690.
<https://doi.org/10.1016/j.cej.2022.134690>
39. Chen X, Han S, Wu W, *et al.*, 2022, Harnessing 4D printing bioscaffolds for advanced orthopedics. *Small*, 18(36):e2106824.
<https://doi.org/10.1002/sml.202106824>
40. Fayyazbakhsh F, Khayat MJ, Leu MC, 2022, 3D-printed gelatin-alginate hydrogel dressings for burn wound healing: A comprehensive study. *Int J Bioprint*, 8(4):618.
<https://doi.org/10.18063/ijb.v8i4.618>
41. Liu Y, Wong CW, Chang SW, *et al.*, 2021, An injectable, self-healing phenol-functionalized chitosan hydrogel with fast gelling property and visible light-crosslinking capability for 3D printing. *Acta Biomater*, 122:211–219.
<https://doi.org/10.1016/j.actbio.2020.12.051>
42. Zhong H, Huang J, Wu J, *et al.*, 2021, Electrospinning nanofibers to 1D, 2D, and 3D scaffolds and their biomedical applications. *Nano Res*, 15(2):787–804.
<https://doi.org/10.1007/s12274-021-3593-7>
43. Wu Z, Hong Y, 2019, Combination of the silver-ethylene interaction and 3D printing to develop antibacterial superporous hydrogels for wound management. *ACS Appl Mater Interfaces*, 11(37):33734–33747.
<https://doi.org/10.1021/acsami.9b14090>
44. Streifel BC, Lundin JG, Sanders AM, *et al.*, 2018, Hemostatic and absorbent polyHIPE-kaolin composites for 3D printable wound dressing materials. *Macromol Biosci*, 18(5):1700414.
<https://doi.org/10.1002/mabi.201700414>
45. Long J, Etxeberria AE, Nand AV, *et al.*, 2019, A 3D printed chitosan-pectin hydrogel wound dressing for lidocaine hydrochloride delivery. *Mater Sci Eng C Mater Biol Appl*, 104:109873.
<https://doi.org/10.1016/j.msec.2019.109873>
46. Zhao X, Li P, Guo B, *et al.*, 2015, Antibacterial and conductive injectable hydrogels based on quaternized chitosan-graft-polyaniline/oxidized dextran for tissue engineering. *Acta Biomater*, 26:236–248.
<https://doi.org/10.1016/j.actbio.2015.08.006>
47. Qu J, Zhao X, Liang Y, *et al.*, 2019, Degradable conductive injectable hydrogels as novel antibacterial, anti-oxidant wound dressings for wound healing. *Chem Eng J*, 362:548–560.
<https://doi.org/10.1016/j.cej.2019.01.028>
48. Chung Y-C, Chen C-Y, 2008, Antibacterial characteristics and activity of acid-soluble chitosan. *Bioresour Technol*, 99(8):2806–2814.
<https://doi.org/10.1016/j.biortech.2007.06.044>
49. Wu L, Wu Y, Che X, *et al.*, 2021, Characterization, antioxidant activity, and biocompatibility of selenium nanoparticle-loaded thermosensitive chitosan hydrogels. *J Biomater Sci Polym Ed*, 32(10):1370–1385.
<https://doi.org/10.1080/09205063.2021.1917813>
50. Xu J, Fang H, Su Y, *et al.*, 2022, A 3D bioprinted decellularized extracellular matrix/gelatin/quaternized chitosan scaffold assembling with poly(ionic liquid)s for skin tissue engineering. *Int J Biol Macromol*, 220:1253–1266.
<https://doi.org/10.1016/j.ijbiomac.2022.08.149>
51. Lim SH, Hudson SM, 2004, Synthesis and antimicrobial activity of a water-soluble chitosan derivative with a fiber-reactive group. *Carbohydr Res*, 339(2):313–319.
<https://doi.org/10.1016/j.carres.2003.10.024>
52. Podstawczyk D, Nizioł M, Szymczyk-Ziolkowska P, *et al.*, 2021, Development of thermoinks for 4D direct printing of temperature-induced self-rolling hydrogel actuators. *Adv Funct Mater*, 31(15):2009664.
<https://doi.org/10.1002/adfm.202009664>
53. Qu J, Zhao X, Liang Y, *et al.*, 2018, Antibacterial adhesive injectable hydrogels with rapid self-healing, extensibility and compressibility as wound dressing for joints skin wound healing. *Biomaterials*, 183:185–199.
<https://doi.org/10.1016/j.biomaterials.2018.08.044>

54. Zhao X, Guo B, Wu H, *et al.*, 2018, Injectable antibacterial conductive nanocomposite cryogels with rapid shape recovery for noncompressible hemorrhage and wound healing. *Nat Commun*, 9:2784.
<https://doi.org/10.1038/s41467-018-04998-9>
55. Liu H, Du YM, Wang XH, *et al.*, 2004, Chitosan kills bacteria through cell membrane damage. *Int J Food Microbiol*, 95(2):147–155.
<https://doi.org/10.1016/j.ijfoodmicro.2004.01.022>
56. Peng Z-X, Wang L, Du L, *et al.*, 2010, Adjustment of the antibacterial activity and biocompatibility of hydroxypropyltrimethyl ammonium chloride chitosan by varying the degree of substitution of quaternary ammonium. *Carbohydr Polym*, 81(2):275–283.
<https://doi.org/10.1016/j.carbpol.2010.02.008>